Journal of Volcanology and Geothermal Research 308 (2015) 142–157

Contents lists available at ScienceDirect

Journal of Volcanology and Geothermal Research

journal homepage: www.elsevier.com/locate/jvolgeores

A model of the geochemical and physical fluctuations of the lava lake at Erebus volcano, Antarctica

Indira Molina [a,*], Alain Burgisser [b,c], Clive Oppenheimer [d]

[a] Instituto Geofísico, Escuela Politécnica Nacional, Aptdo. Postal 17-01-2759, Quito, Ecuador
[b] CNRS, ISTerre, 73,376 Le Bourget du Lac, France
[c] Université Savoie Mont Blanc, ISTerre, 73376 Le Bourget du Lac, France
[d] Department of Geography, University of Cambridge, Downing Place, Cambridge CB2. 3EN, UK

ARTICLE INFO

Article history:
Received 23 April 2015
Accepted 31 October 2015
Available online 10 November 2015

Keywords:
Magma convection
Volcanic gas fluxes
Degassing
Conduit
Erebus

ABSTRACT

Erebus volcano, Antarctica, exhibits periodical surface fluctuations of both geochemical and physical nature. Modeling the physics driving the lake oscillation is a challenge, even with a relatively simple theoretical framework. We present a quantitative analysis that aims to reconcile both lake level and gas geochemical cycles. Our model is based on the assumption that the periodicity is caused by the regular release of magma batches and/or core annular flow that have a fixed volume of melt and ascend and degas in equilibrium. Results suggest that cycles are not caused by the mixing between magma residing in the lake and a deep magma but by two distinct deep sources that rise separately. These sources of bubbly magma come from at most 2–3 km depth and rise buoyantly. Individual batches detach from the rising magmas at depths of 20–250 m. The two batch types can coexist in a single conduit up to a depth of ~30 m, above which they rise alternately to release respectively 19 and 23 kg/s of gas at the lake surface every 10 min. The temperature of the descending flow is between 890 and 950 °C, which is roughly 100 °C colder than the ascending currents. Batch pairs have shapes likely constrained by the conduit width. Regardless of their shapes, the pairs reach very high porosities near the surface and have diameters of 4–14 m that are consistent with video observations showing spreading waves at the lake surface. The alternating arrival of these large batches suggests a lava lake mostly filled with gas-rich magma.

1. Introduction

The lava lake in the summit crater of Erebus volcano, Antarctica, has sourced a persistent gas plume for at least several decades. This overall longevity is accompanied by a series of cyclical processes that also persist. These include cyclic change in the level of the lava lake. These periodic variations are remarkably in phase with changes in the respective proportions of different gases in the plume, variation of the heat loss and gas temperature at the surface of the lake, and changes of the surface velocity of the magma (Oppenheimer et al., 2009; Alletti et al., 2014; Peters et al., 2014a,b; Jones et al., 2015). The duration of these various cycles – approximately 10–20 min – is stable to first order over the years (Oppenheimer et al., 2009; Peters et al., 2014b; Ilanko et al., 2015a).

Focusing on the lava lake level, the amplitude of the pulsation is ~1.5 m, with sporadic fluctuations up to ~3 m (Peters et al., 2014b). This short term pulsation has been described as a cyclic process starting with a steady uplift of the magma surface which exposes a greater proportion of incandescent magma at widening cracks and reaching a peak accompanied by maximum gas flux (Oppenheimer et al., 2009; Boichu et al., 2010; Peters et al., 2014b). The lake level then falls to its previous value. These cycles do not affect measurably the lake surface area, which changes over longer timescales. For instance, the lake area, has ranged between ~500 and ~2000 m^2 over the period 2001–2013 (Fig. 5 from Sweeney et al., 2008; Peters et al., 2014b; Jones et al., 2015). Those changes have been associated with secular change in lake level (Jones et al., 2015) but do not affect the 10–20 min period oscillations (Peters et al., 2014a).

The most commonly invoked mechanism to explain the oscillatory behavior of Erebus lava lake is the presence of instabilities in the bidirectional flow occurring in the conduit feeding the lake (Oppenheimer et al., 2009; Molina et al., 2012; Peters et al., 2014a). Our objective is to construct simple physical scenarios of unstable, bidirectional conduit flow to assess whether that general mechanism can explain these oscillations. Our effort joins a series of studies aimed at explaining the physical mechanisms of magma degassing at persistently active volcanoes (e.g., Kazahaya et al., 1994; Stevenson and Blake, 1998; Witter et al., 2005; Witham and Llewellin, 2006; Witham et al., 2006; Palma et al., 2011; Beckett et al., 2014). The physical scenarios are constrained by data collected in 2004 and reported by Oppenheimer et al. (2009)

* Corresponding author.
E-mail address: indimolina08@gmail.com (I. Molina).

http://dx.doi.org/10.1016/j.jvolgeores.2015.10.027
0377-0273/

(height, duration of the oscillation and gas flux measurement) and on the equilibrium temperatures of the gas (Burgisser et al., 2012). The model runs predict conduit sizes that are compared with independent estimates. Along with coherent physical templates, successful runs yield estimates of the temperature contrast between the ascending and descending currents.

Our model starts from the flow instability hypothesis by considering the rise of magma batches caused by the breakdown of the instabilities. These batches ascend in the conduit by buoyancy due to porosity and temperature contrast between ascending and descending currents in such a way that they yield a surface gas flux that matches the observed values. Batch dynamics are based on Kazahaya et al. (1994), but we consider additionally changing vesicularity due to gas decompression of the ascending magma under equilibrium conditions. Following Stevenson and Blake (1998) and Beckett et al. (2014), we investigate whether the degassing-induced convection provides an efficient mechanism for gas release at shallow levels as a function of the volatile budget associated with the deeper part of the magma system. The main difference with Stevenson and Blake (1998) is that our gas phase is multi-component (nine molecular species) (Burgisser et al., 2012, 2015), and the rheological properties of the ascending and descending currents are temperature-dependent and time-space dependent along the path between the deeper region of the magma system and the lake surface. In contrast to the case of Stromboli (Beckett et al., 2014), crystallization of magma in the conduit is assumed to be negligible (Moussallam et al., 2015).

We present lake elevation changes derived from infrared data collected at the end of 2009, which complement Terrestrial Laser Scanning (TLS) data from 2009–2010 (Jones et al., 2015) and 2012 (Peters et al., 2014b), and which we use to constrain the physical modeling of the shallow part of the Erebus magmatic system. The assumed physics of magma ascent in discrete batches or as a core-annular flow is then explained, and the resulting physical models are combined in four scenarios aimed at reproducing the lake level oscillations. Results from model runs are then used to consider the plausibility of these scenarios and to quantify the likely temperature differences of the ascending and descending flows as well as the likely porosities of the batches when they reach the surface.

2. Methods

2.1. Field data on height oscillations

The data presented here were collected in December 2009 and 2010 during the austral summer field season on Erebus volcano. Time series of thermal imagery were acquired with a FLIR Systems™ ThermaCAM P25 infrared camera (Peters et al., 2014a). The instrument's detector consists of a focal plane microbolometer array composed of 320 × 240 elements and is sensitive in the 7.5–13 μm waveband. The camera was firmly affixed to a tripod positioned on the crater rim at a site known as Shackleton's Cairn. The lava lake was approximately 220 m vertically below the monitoring site. A 72 mm focal length lens was attached to the fore-optics, which yielded a tight frame around the lava lake whose perimeter in December 2009 lay between approximately 315 and 350 m line of sight from the camera. The nominal instantaneous field of view (IFOV) of the system is 0.625 μrad and the viewing geometry corresponded to a footprint of each detector element of approximately 0.2 m projected to the wall of the pit crater containing the lava lake. Time-stamped images were recorded continuously and automatically on to a flash memory card housed in the camera roughly every 16 s. Replaying the time series of imagery at a rapid frame rate immediately reveals the surface motion of the lava lake. Of particular note is variation in the lake level, a quantitative time-series of which was acquired.

We estimated the lake level by visually tracking the rise and fall of the lake margin at the far wall of the pit crater containing the lake. The lake margin is identified by the sharp thermal contrast between lake surface and pit wall. We recorded lake height frame-by-frame using the known optical path (350 m) and IFOV of the camera to provide a distance scale. This procedure is similar to that used to monitor the level of the summit lava lake at Kīlauea volcano (Patrick et al., 2014). This was straightforward for rising lake level but more challenging for the subsiding surface due to a reduced thermal contrast between lake surface and pit wall. Based on the image spatial resolution, we consider the precision on these measurements to be of order ±0.2 m.

2.2. Pre-conceptual physical template of Erebus plumbing system

Our modeling requires knowledge of the plumbing system geometry and constraints on magma temperature and crystal contents. During the 1987/1988 season, after a Strombolian explosion had evacuated the lava lake, Dibble et al. (2008) observed a funnel-shaped floor as deep as its width, with a hole (uppermost conduit) whose diameter was about half that of the full lake. There are no reports of the lake area for that particular season, however in 1989, McClelland et al. (1989) reported a satellite image based estimate of 300 m^2. Assuming that during 1987/1988 season the lake had 300 m^2 and was circular, the lake diameter would be 20 m and the conduit diameter therefore about 10 m Numerical simulations for Erebus phonolitic magma suggest that a conduit of at least 10 m is needed to sustain convection between the lake and a deeper reservoir (Molina et al., 2012). The lake is estimated to be at least 20 m deep (Aster et al., 2003; Oppenheimer et al., 2009).

Geochemical and physical observation of the lava lake in December 2004 revealed cyclically varying gas composition and flux (Oppenheimer et al., 2009; Ilanko et al., 2015a). Taking the 2004 data as a baseline, we assume that the cycles are caused by the periodic release of distinct gas sources into the lake so that the modal period is about 10 min (Fig. 1a). Following Oppenheimer et al. (2009), the source causing the lowest flux in the cycle (~19 kg/s) is composed of "conduit gas". The source with the highest flux (~23 kg/s) can be of two origins. It could be distinct from the conduit gas, in which case it is composed of "top gas". It could, on the other hand, result from the superposition of the conduit gas with a "lake gas" originating from the lava lake itself (Oppenheimer et al., 2009). In the latter case, the lake gas has a flux corresponding to the difference between the highest and lowest gas fluxes (~4 kg/s). One hypothesis we tested is whether oscillations are due to a combination of two alternating sources of "top gas" and "conduit gas", or if they are caused by discrete releases of "lake gas" overprinting a continuous flux of "conduit gas".

Burgisser et al. (2012), Alletti et al. (2014), and Ilanko et al. (2015a) found through thermodynamical modeling of gas compositions typical of the highest and lowest gas fluxes that they are associated with different equilibrium temperatures. Briefly, the chemical model of Burgisser et al. (2012) uses four measured gas species ratios at the vent (CO_2/CO, CO_2/H_2O, CO_2/SO_2, and SO_2/OCS) and calculates at atmospheric pressure the equilibrium temperature and the other gas species that are in equilibrium with the measured species. This calculation yields the gas composition (H_2O, H_2, O_2, SO_2, H_2S, S_2, CO_2, CO, and CH_4) at the vent. Focusing on December 2005, the "top gas" would be generated at temperature conditions at the lake surface of 1084 °C, the "conduit gas" at 1069 °C (Burgisser et al., 2012). According to the same chemical model, the

"lake gas" composition calculated by Oppenheimer et al. (2009) equilibrated at 1015 °C. The chemical composition of these three gas types is given in Table 1.

The chemical model of Burgisser et al. (2012) calculates the isothermal evolution with increasing pressure of the partition of the volatile species between the gas and the melt. For a given proportion of gas and melt, the model simulates a closed-system compression from atmospheric pressure to the pressure at which the amount of gas phase vanishes because all volatiles are dissolved into the melt. The species dissolved in the melt are H_2O, CO_2, H_2, and S. Thus, for an initial surficial gas composition and gas fraction, the average molar mass of the gas phase, M_{avg}, the melt water content, and the total gas weight fraction, W_{gT}, are calculated as a function of confining pressure P.

The geochemical and physical evidence presented above allows us to postulate that magmas with different gas compositions reach the lake surface in the form of "batches" (spherical or spheroidal) or "continuous flow" (Poiseuille flow) of a given gas content (or porosity) and cause the oscillations. We will treat independently the physics associated with each type of batch (sphere or spheroid) or a continuous flow in the next section. We constrain our modeling by the following parameters or criteria:

(1) A lake depth of ~20 m (Aster et al., 2003; Oppenheimer et al., 2009) and conduit diameter of at least 10 m (e.g., Dibble et al., 2008; Molina et al., 2012) and as much as 20 m.
(2) Two batches/flows cannot collide or occupy the same space; however they can be at the same depth if the size of the plumbing system allows. Batches do not interact, mix or merge, therefore, batches of the same composition and porosities will be separated above a "*detachment depth*" at which they behave independently or as isolated batches (i.e., when the distance between identical batches exceeds the batch radius). Batches of different compositions can coexist side by side above a "*generation depth*" if the geometry of the plumbing system allows. In narrow conduits, the "*generation depth*" lies at the point where the distance between adjacent batches of different composition exceeds the average batch radius. Below the "*generation depth*", our model finds its limits because our calculations assume individual batches.
(3) The emitted minimum and maximum gas fluxes of 19 and 23 kg/s, respectively (Oppenheimer et al., 2009).
(4) A variation of lake level corresponds to the release of the equivalent volume of gas as a direct result of the accumulation of gas below the surface.

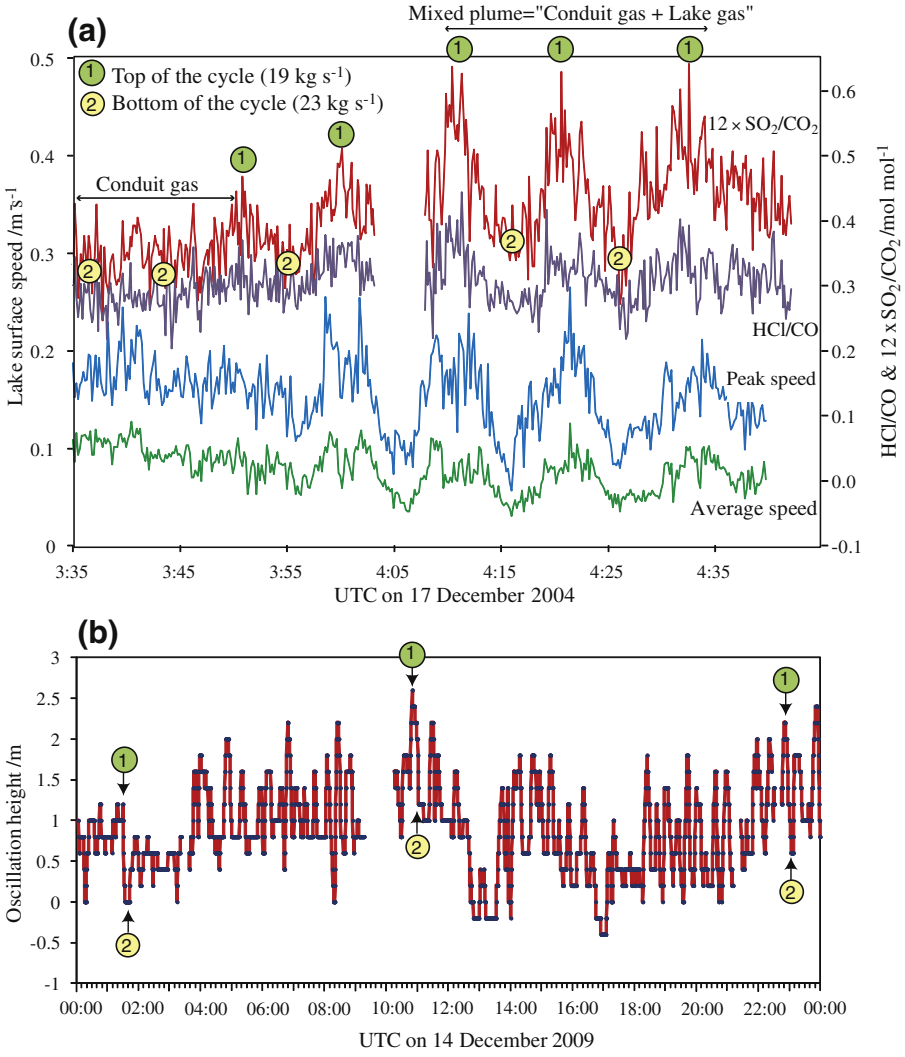

Fig. 1. Time series at Erebus lava lake for: (a) geochemical and average speed data in December 2004 (modified from Oppenheimer et al., 2009). (b) Surface height oscillations in December 2009 (times are UTC). Each division on the *x* axis represents 10 min. Labels 1 and 2 refer to examples of the geochemical and flux signatures of the high- and low-ends of the gas flux cycles.

Table 1
Initial conditions at $P = 0.065$ MPa for the three gas types. Gas species OCS is neglected in all runs due to its small influence on the results and the large uncertainty on its behavior at high pressure (Burgisser et al., 2012). NA means not applicable. M_{av} is the average molecular weight, W_{gT} is total gas weight fraction, and ϕ is the gas volume fraction.

Gas species (mol fraction)/parameter	Top gas[a]	Conduit gas[a]	Lake gas[b]
H_2O	0.730	0.555	0.859
H_2S	0.002	0.002	0.034
SO_2	0.011	0.009	0.025
H_2	0.024	0.020	0.037
O_2	7.9×10^{-11}	3.95×10^{-11}	4.12×10^{-11}
S_2	1.4×10^{-4}	1.7×10^{-4}	0.9×10^{-4}
CO	0.014	0.027	0.0025
CO_2	0.219	0.388	0.034
CH_4	9.8×10^{-6}	$1.8 \times 1\,0^{-5}$	1.8×10^{-5}
Melt H_2O (wt.%)	0.0229	0.019	0.0256
M_{avg}(kg/mol)	0.030	0.035	0.026
W_{gT} @ = 0.1 (wt. fract.)	7.0×10^{-4}	9.0×10^{-4}	6.5×10^{-4}
W_{gT} @ = 0.2 (wt. fract.)	1.6×10^{-3}	1.9×10^{-3}	1.4×10^{-3}
W_{gT} @ = 0.3 (wt. fract.)	2.7×10^{-3}	3.2×10^{-3}	2.5×10^{-3}
W_{gT} @ = 0.4 (wt. fract.)	4.2×10^{-3}	5.0×10^{-3}	3.8×10^{-3}
W_{gT} @ = 0.5 (wt fract.)	6.3×10^{-3}	7.4×10^{-3}	5.7×10^{-3}
W_{gT} @ = 0.6 (wt fract.)	9.5×10^{-3}	1.1×10^{-2}	8.5×10^{-3}
W_{gT} @ = 0.7 (wt fract.)	1.5×10^{-2}	1.7×10^{-2}	1.3×10^{-2}
Equilibrium temperature (°C)	1084	1069	1015
Measured flux (kg/s)[c]	23	19	NA
Deducted flux (kg/s)[c]	NA	NA	4

[a] Gas composition from Burgisser et al. (2012).
[b] Partial lake gas composition (CO_2/CO, CO_2/H_2O, CO_2/SO_2, and SO_2/OCS) was estimated by Oppenheimer et al. (2009) by difference using the composition and fluxes of the top gas and the conduit gas. Other species were calculated using the model of Burgisser et al. (2012).
[c] Values from Oppenheimer et al. (2009).

(5) The lake dynamics are dominated by arrival of magmas with different porosities in the form of "batches" (sphere or spheroid) and/or "continuous flow" (Poiseuille flow).
(6) Gas temperatures are represented by equilibrium temperatures calculated by the model of Burgisser et al. (2012).
(7) The gas hosted in the batch is composed of nine chemical species and the melt contains four dissolved species. Runs of the chemical model of Burgisser et al. (2012) yield M_{avg}, the melt water content, and W_{gT} as a function of P (Table 1).

As magma batches rise at different speeds, they can reach the lake surface either perfectly synchronized, or alternately. We consider that the lake oscillations could arise from four different scenarios (i.e. cyclic behaviors) illustrated in Fig. 2:

Scenario 1 Explains the oscillations by the alternating arrival of spherical batches reaching the surface every 10 min and shifted in time by 5 min. Each batch type emits a respective gas flux of 19 kg/s (conduit gas) and 23 kg/s (top gas) and the arrival of every batch causes an oscillation of the lava lake level when reaching the surface.
Scenario 2 Explains the low-flux endmember as the succession of batches with "conduit gas" composition reaching the surface every 5 min. The high end of the flux reflects the addition of batches with "lake gas" composition reaching the surface every 10 min. Each batch type emits a respective gas flux of 19 and 4 kg/s and the arrival of every other batch causes an oscillation when reaching the surface. As a result, the non-occurrence of the lake gas batch results in the sole release of the conduit (see scenario 3).
Scenario 3 Explains the low-flux endmember as a continuous flow (Poiseuille-type) with "conduit gas" composition on which the periodical arrival of batches with "lake gas" composition is superimposed every 10 min. The arrival of the lake gas batches with a flux of 4 kg/s cause the oscillations. In this scenario, the fluctuation is not seen as the succession of alternating batches but as the repetitive occurrence of batches with composition "lake gas".
Scenario 4 Similar to scenario 1 in that it explains the oscillations by the alternating arrival of conduit gas and top gas batches reaching the surface every 10 min and shifted in time by 5 min. The assumption of spherical batches is relaxed so that batches can be constrained by the conduit diameter to become spheroidal.

The volumetric magma flux of an unsteady bi-directional flow can be calculated by two end-member fluid dynamics models. The first model corresponds to Stokes flow in which a sphere of degassing magma rises in a cylindrical conduit or in which spheroids of degassing magma with a fixed horizontal diameter rise up the conduit. This model is valid for viscous spheres rising within an incompressible fluid. The second model is Poiseuille flow through a double concentric pipe in which a less viscous and less dense magma ascends in the core and a more viscous, denser magma descends in the outer part along the conduit walls. This model is only valid for incompressible fluids.

2.3. Stokes approximation of magma batch ascent

Among others, Koyaguchi (1985) and Palma et al. (2011) experimentally observed that miscible liquids can rise in batches. We consider that these batches include melt and gas and have a spherical to spheroidal geometry. We used the derivation of Stokes' theory used by Kazahaya et al. (1994) and McNown and Malaika (1950) to calculate the velocity of the rising batch. The difference with Kazahaya's treatment is the presence of bubbles in a sphere (Fig. 3) and the possibility of having a batch with spheroidal (an ellipsoid with two equal semi-diameters) or prolate geometry (elongated vertically).

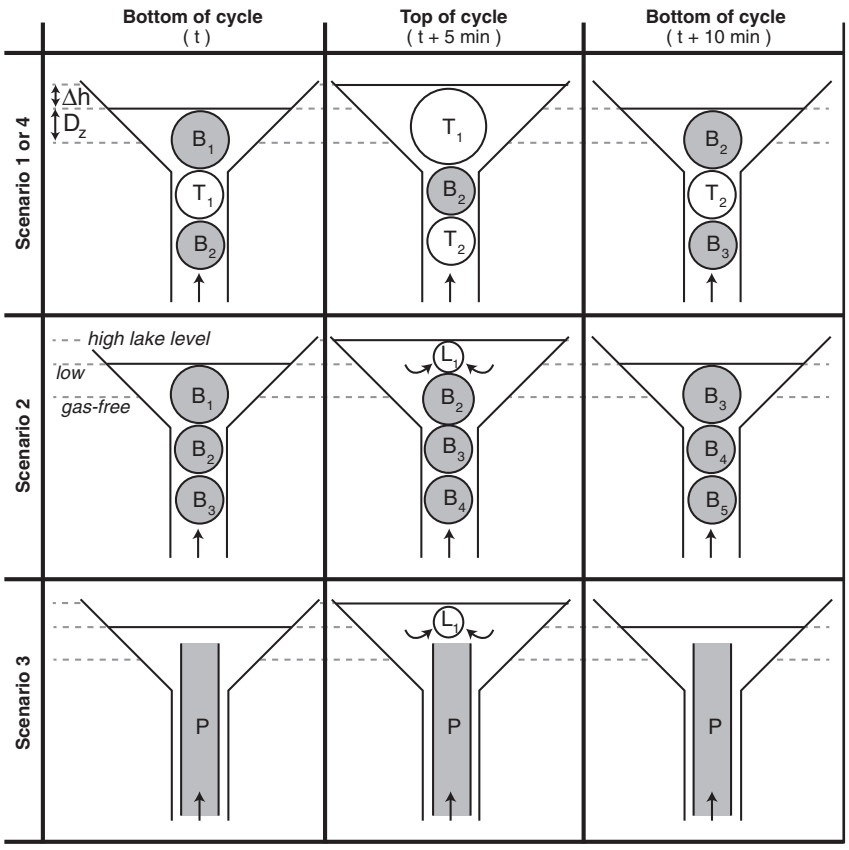

Fig. 2. Schematic cross sections of the lava lake and the upper part of its feeder conduit illustrating the four degassing scenarios analyzed in this study. Scenarios 1 and 4 depict the alternate arrival every 10 min of spherical (scenario 1) or spheroidal (scenario 4) batches of top (labels T_{1-2}) and conduit (labels B_{1-3}) gas compositions. Scenario 2 depicts the arrival every 5 min of spherical batches with conduit gas composition (labels B_{1-5}) and superimposition ever 10 min of batches with lake gas composition (label L_1). Scenario 3 depicts continuous flow with conduit gas composition (label P) and superimposition every 10 min of batches with lake gas composition (label L_1). The variable D_z measures the height gain due to the gas contribution at the low end of the flux cycle (label "low") with respect to a gas-free lake level (label "gas-free"). The value of Δh corresponds to the height amplitude of the cycle that brings the lake level to its highest position (label "high lake level").

Fig. 3 depicts a batch of density ρ_{blob}, viscosity μ_{asc}, temperature T_{asc}, porosity ϕ (made of gas of specific composition with a molecular average, M_{avg}, and weight fraction, W_{gT}), hosting a crystal-bearing, hydrous melt of density ρ_{asc} rising with a velocity U_{batch} within an incompressible, crystal-bearing, anhydrous melt of density ρ_{desc}, viscosity μ_{desc} and temperature T_{desc}. The batch has three principal axes: two radii of the same magnitude in the equatorial plane that we call $R_{x\ batch}$ and $R_{y\ batch}$, respectively, and an axis in the z-direction $R_{z\ batch}$. For spherical geometries, $R_{x\ batch} = R_{y\ batch} = R_{z\ batch}$ evolves as a function of depth, z, as the result of the expansion of the gas hosted within the batch, while for spheroidal geometries the axes $R_{x\ batch} = R_{y\ batch}$ are fixed while $R_{z\ batch}$ accommodates the gas expansion mentioned above. We call $R_{x\ batch} = R_{y\ batch} = R_{batch}$ and we use it as the nominal radius which is that of a sphere of the same volume as in McNown and Malaika (1950).

The pressure, P, is a sole function of depth, so that descending fluid and rising batches have equal pressures when located at the same depth. We discretized our domain in space (the vertical axis z is positive downwards) as follows:

$$z = \frac{P - P_{atm}}{\rho_{desc} g} \tag{1}$$

where z is the depth of the batch (center of the sphere), P is the hydrostatic pressure at depth z due to the melt surrounding the batch, P_{atm} is the local atmospheric pressure at 0.065 MPa and g is the gravitational constant. The maximum difference in crystal content, ε_s, between the ascending and descending melts being about 4 vol.% (Molina et al., 2012), we assume it as constant and equal to 30 vol.% (Kelly et al., 2008). The descending melt density, ρ_{desc}, is calculated with Conflow (Mastin and Ghiorso, 2000) by fixing the descending temperature, T_{desc}, the phonolitic melt composition in major oxides, the properties of the 30 vol.% of anorthoclase crystals and a water content of 0 wt.%. It is taken as a constant along the conduit.

At low pressure, we can approximate the density of gas, ρ_{gas}, as a function of pressure by applying the ideal gas law:

$$\rho_{gas}(z) = \frac{P\, M_{avg}}{R\, T_{asc}} \tag{2}$$

where R is the universal constant gas law (8.314 J/K mol). The volume of gas in the batch, V_g, is thus a function of depth:

$$V_g(z) = \begin{cases} V_{go},\ z = 0 \\ V_{go} \dfrac{\rho_{gas}|_{z=0}}{\rho_{gas}|_z},\ z > 0 \end{cases} \tag{3}$$

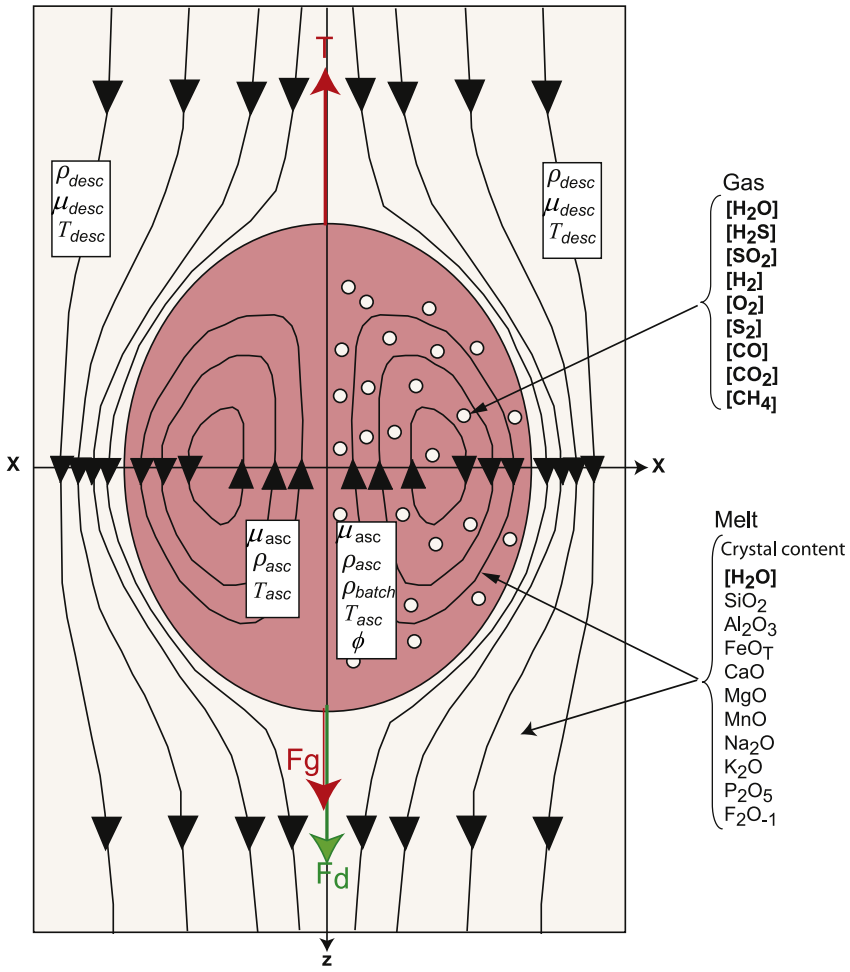

Fig. 3. Sketch of streamlines in and around a viscous sphere containing silicate melt and crystals (dark red) and gas bubbles (white) and moving through a Newtonian fluid containing silicate melt and crystals (light red) (redrawn from Weinberg and Podladchikov, 1994). Melt composition is constant except for melt H_2O content. Gas composition varies as a function of depth. Arrows represent the main forces acting on the sphere (body forces in red and surface force in green).

where the initial gas volume, V_{go}, is given by the surface of the lake, S, multiplied by an equivalent height. This equivalent height depends on the position of the lake surface within the oscillation cycle. Batches responsible for the low end of the flux cycles have an initial volume $V^b_{g0} = SD_z$ and batches associated with high gas fluxes have an initial volume $V^t_{g0} = S(D_z + \Delta h)$. This formulation means that D_z corresponds to the height due to the gas volume fraction present within the lake during the low end of the cycle with respect to a gas-free lake and that Δh corresponds to the amplitude of the cycle (Fig. 2).

Following Burgisser et al. (2008), the gas volume fraction, ϕ, of any ascending batch can be calculated at each depth according to:

$$\phi(z) = \left[1 + \frac{M_{avg}\, P\, (1 - W_{gT})}{R\, T_{asc}\, \rho_{asc}\, W_{gT}}\right]^{-1} \tag{4}$$

where ρ_{asc} is the density of hydrous melt inside the batch calculated with Conflow (Mastin and Ghiorso, 2000) by fixing the ascending temperature, T_{asc}, the phonolitic melt composition (major oxides) (mean values reported in Table 2 from Kelly et al., 2008), the properties of 30 vol.% of anorthoclase crystals (Table A1 from Molina et al., 2012), and the melt water content at $z = 0$ using the chemical model of Burgisser et al. (2012) (Table 1). The density calculation assumes a constant value for melt water content in the ascending flow as its variation induces negligible density changes compared to those induced by porosity variations. As it ascends, the batch grows because of gas expansion. The melt is taken as incompressible so that it is displaced by the expanding gas. We obtain the constant volume of melt with:

$$V_{melt} = V_{go}\left(\frac{1}{\phi|_{z=0}} - 1\right). \tag{5}$$

By combining Eqs. (3) and (5) we calculate the total volume of the batch (melt plus gas), and derive its nominal radius R_{batch}, and hence its radius in the z-direction $R_{z\ batch}$:

$$R_{batch}(z) = \sqrt[3]{\frac{3}{4\pi}\left[V_g(z) + V_{melt}\right)} \tag{6a}$$

$$R_{z\,batch}(z) = \frac{3}{4\pi}\frac{[V_g(z) + V_{melt})]}{R_{batch}^2}. \tag{6b}$$

Viscosity is a key parameter influencing magma motion that heavily depends on the temperature and on the crystal and bubble contents (e.g. Petford, 2009). The relationship to calculate the effective dynamic viscosity of the magma, μ_m, was obtained by multiplying the relative contributions provided by three phases: melt, crystals and bubbles. The viscosity of the melt is obtained through the VFT equation (Giordano et al., 2008; Le Losq et al., 2015), which is a function of temperature and of the major oxides including dissolved water. Since dissolved H_2O varies as a function of depth, we varied the B and C coefficients of the VFT equation accordingly (see Eq. (11) in Molina et al. (2012)). Melt viscosity was adjusted to take into account the presence of crystals using the relationship proposed by Krieger and Dougherty (1959) (see Eq. (2) in Molina et al. (2012)). Following Shimozuru (1978), the bulk viscosity increases with the presence of gas bubbles and the term $(1 + (z))$ was added under the assumption of a small Reynolds number to yield the following expression:

$$\mu_m = \begin{cases} \mu_{asc}(z) = \left[10\exp\left(A + \frac{B}{T_{asc} - C}\right)\right][1 + \phi(z)]\left[1 - \frac{\varepsilon_s}{1-\varepsilon_m^*}\right]^{-[\eta](1-\varepsilon_m^*)} \\ \mu_{desc} = 10\exp\left(A + \frac{B}{T_{desc} - C}\right)\left[1 - \frac{\varepsilon_s}{1-\varepsilon_m^*}\right]^{-[\eta](1-\varepsilon_m^*)} \end{cases} \tag{7}$$

where $A = -4.55$ is a coefficient independent of composition, $\varepsilon_s = 0.3$ is the crystal fraction, $\varepsilon_m^* = 0.35$ is the void fraction at maximum packing of crystals (implying that this void is filled by melt), and $[\eta] = 2.5$ is the Einstein coefficient (a value for the bulk viscosity for rigid sphere – crystal – suspension if there is no slippage of liquid at the interface). The descending melt is assumed anhydrous and bubble-free.

2.3.1. Terminal velocity of ascending batches

To account for internal as well as the external motion in a viscous sphere rising in a still fluid, Hadamard and Rybczynski defined the drag forces acting on the sphere as the product between the buoyancy force acting on a solid sphere, $6\pi R_{batch}U_{batch}$, which is well-known as Stokes law (Lamb, 1945, p. 598) and the ratio of viscosities between the ascending sphere and the descending fluid, $(2\mu_{desc} + 3\mu_{asc})/(3\mu_{desc} + 3\mu_{asc})$ (Lamb, 1945, p. 601). This approximation neglects surface tension and inertial forces and is valid for laminar flow (particle Reynolds number, Re, lower than 1). For increasing Re, inertial forces become more important and can be, to first order, be approximated using Oseen's multiplicative factor to the drag forces defined by Stokes, $(1 + 3/16\,Re)$ (Lamb, 1945, p. 617). This approximation is valid for $Re < 5$ (Crowe et al., 1997). Later, Kazahaya et al. (1994) combined these works to define a more complete expression of the drag force acting in a moving viscous sphere through an infinite Newtonian fluid. In contrast, McNown and Malaika (1950) extended Stokes law for solid particles of any shape introducing two shape factors α and β that account for the principal axes of particles with a nominal radius R_{batch}, $6\pi R_{batch}U_{batch}[16/6R_{batch}(\alpha + \beta)]$. As surface tension is negligible because our ascending and descending fluids are miscible silicate melts, we combine Kazahaya et al. (1994) and McNown and Malaika (1950) approximations to quantify the total force required maintaining steady-state flow as follows:

$$\overbrace{\frac{4}{3}\pi R_{z\,batch}R_{batch}^2(\rho_{desc} - \rho_{batch})g}^{\text{Excess of buoyancy of the spheroidal batch over its gravity}} - \overbrace{6\pi R_{batch}U_{batch}\mu_{desc}}^{\text{Resistance of a solid sphere}}\overbrace{\frac{2\mu_{desc} + 3\mu_{asc}}{3\mu_{desc} + 3\mu_{asc}}}^{\text{viscous sphere}}\overbrace{\left(1 + \frac{3}{16}Re\right)}^{1^{st}\text{order inertia}}\overbrace{\left(\frac{16}{6R_{batch}(\alpha + \beta)}\right)}^{\text{spheroidal batch}} = 0 \tag{8}$$

where U_{batch} is the terminal velocity of the batch, R_{batch} is the nominal radius of the batch, $R_{z\,batch}$ is the batch radius in the z-direction. In the case of a spherical batch $R_{z\,batch} = R_{batch}$. Re is the batch Reynolds number defined as:

$$Re = \frac{2R_{batch}U_{batch}\rho_{desc}}{\mu_{desc}} \tag{9}$$

and the density of the batch, ρ_{batch}, is:

$$\rho_{batch}(z) = \phi\rho_{gas} + (1 - \phi)\rho_{asc}. \tag{10}$$

The geometrical factors, α and β, for a prolate spheroid and for a sphere are defined in Appendix A (McNown and Malaika, 1950). Considering a cylindrical shell coincident with the circular section of the sphere, we can calculate the total gas flux reaching the surface, Q_{g_St}, by not including the crystals and melt fraction contained in the batch:

$$Q_{g\_St} = \pi R_{batch}^2 U_{batch}\,\phi\rho_{gas}. \tag{11}$$

2.4. Poiseuille approximation for core-annular flow

The volumetric flow rate of magma of viscosity μ_{asc} through a cylindrical conduit is the total volume of fluid passing across any section per unit of time:

$$Q_{v\_p} = \frac{R_c^4}{8\mu_{asc}}\frac{dP}{dZ} \tag{12}$$

Following Kazahaya et al. (1994), we consider that the ascending fluid is the center part of a core annular flow. R_c is the core radius and dP/dZ is the pressure gradient that drives magma ascent. The differential buoyancy of the ascending core relative to the descending annulus of magma is given by

$dP/dZ = (\rho_{desc} - \rho_{core})g$. From Eq. (12), the mass of gas reaching the surface as a "continuous flux" is calculated without considering the crystals and melt fraction in the batch:

$$Q_{g\_p} = \frac{\pi(\rho_{desc} - \rho_{core})gR_{core}^4}{8\mu_{asc}}\ \phi\rho_{gas} \tag{13}$$

where the ascending magma density is calculated as for a batch ($\rho_{core} = \rho_{blob}$) and the core radius R_{core} is constant. The velocity of the core, U_{core}, is calculated as the volume flux passing through a flat spherical shell as $U_{core} = [(\rho_{desc} - \rho_{core})gR_{core}^2]/(8\mu_{asc})$. The magma ascent rate is calculated as for the batch by replacing U_{batch} by U_{core} in Eq. A4 (Appendix A).

2.5. Conduit radius

Stevenson and Blake (1998) indicates that conduit radius, R_c, can be inferred by a Poiseuille number, P_s, the terminal velocity of ascending magma, U_{asc} (we take $U_{asc} = U_{batch}$, which draws an equivalence between batches and core-annular flow in agreement with Kazahaya et al. (1994)) and the difference in density between the degassed and gas-rich magmas ($\Delta\rho = \rho_{batch} - \rho_{desc}$ in our case). The value of P_s is a function of μ_{desc}/μ_{asc} based on their experiments; if $1 < \mu_{desc}/\mu_{asc} < 12$ then $P_s = 0.020 + 0.041\ \log_{10}(\mu_{desc}/\mu_{asc})$, and if $\mu_{desc}/\mu_{asc} > 12$ then $P_s = 0.064$. Stevenson and Blake (1998) propose that the conduit radius is given by:

$$R_c = R_{c\,max} = \left(\frac{U_{asc}\,\mu_{desc}}{g\,\Delta\rho P_s}\right)^{1/2}. \tag{14a}$$

This equation gives an estimate of the conduit radius based on the maximum flux, which we term $R_{c\ max}$. We also deduce a minimum conduit radius, $R_{c\ min}$, based on the volume brought by a batch/flow in the time interval T between batches/flow of the same composition. If we express $U_{asc} = (V_{melt} + V_g)/(\pi R_c^2 T)$, the minimum conduit radius is:

$$R_{c\,min} = \left[(V_{melt} + V_g)\mu_{desc}/\pi T g\,\Delta\rho P_s\right]^{1/4}. \tag{14b}$$

2.6. Method of solution

Our aim is to investigate how a fluid dynamics model linked to the chemical model of Burgisser et al. (2012) can explain the gas fluxes estimated by Oppenheimer et al. (2009). Our first method of solution is to pair two alternating magma batches of different compositions (respectively "conduit gas" with "top gas" and "conduit gas" with "lake gas") and porosities (scenarios 1, 2, and 4; Table A1 with the online version of the paper). We fix the initial value of ascending temperature, T_{asc}, for each batch in agreement with the equilibrium temperature given in Table 1 and use outputs of the chemical model of Burgisser et al. (2012) to pre-calculate values of M_{avg}, W_{gT}, and melt H_2O content as function of pressure for seven initial gas contents (Table 1). By combining Eqs. (2), (4), (6a), (A2) and (11), and after algebraic arrangement (Appendix A), the gas flux released by a batch with spherical or spheroid geometries at the surface becomes:

$$Q_{g\_St} = \frac{4}{3}\pi R_{batch}\frac{PM_{\alpha vg}\rho_{\alpha sc}W_{gT}}{RT_{\alpha sc}\rho_{asc}W_{gT} + PM_{\alpha vg}(1-W_{gT})}\frac{\sqrt{(\mu_{desc}M)^2 + \frac{3}{8}R_{z\,batch}R_{batch}^3\rho_{desc}(\rho_{desc}-\rho_{batch})gM(\alpha+\beta)} - \mu_{desc}M}{\rho_{desc}M}. \tag{15}$$

Eq. (15) is applied for each batch type, which yields two equations that are linked by the initial values of R_{batch} by using Eq. (6a) and the two measures, D_z and Δh, of equivalent height of the lake level due to the respective gas contributions of each batch type:

$$D_z = \frac{V_{g0}^b}{V_{g0}^t + V_{g0}^b}\Delta h. \tag{16}$$

With Δh specified, three variables are adjusted numerically until the calculated fluxes Q_{g_St} match the observed fluxes (Table 1). This is done by iteratively calculating: (1) the descending temperature, T_{desc}, which is equal for the two alternating batches, (2) the lake level, D_z, and (3) the batch radius, R_{batch}. From these three variables, all the other variables can be calculated at each depth increment. The pre-calculated run of the chemical model gives M_{avg}, W_{gT}, and melt H_2O content as a function of P, ρ_{gas} is obtained from Eq. (2), V_g from Eq. (3), ϕ from Eq. (4), V_{melt} from Eq. (5), R_{batch} from Eq. (6a) in the case of spherical batch or the paired spheroidal batch, $R_{z\ batch}$ from Eq. (6b), μ_{asc} and μ_{desc} from Eq. (7), ρ_{desc} and ρ_{asc} from Conflow, U_{batch} from Eq. (A2), and ρ_{batch} from Eq. (10), respectively. If batches are spheroids, their horizontal radii R_{batch}^t, and R_{batch}^c are fixed.

The second method of solution consists in pairing a continuous Poiseuille flow with periodically superimposed spherical batches (Fig. 2). We use the initial values of Table 1 to assign the respective ascending temperatures, T_{asc}, of the continuous flow and the periodic batches. As in the case of two batches, the values of ($z = 0$) and Δh are set and T_{desc}, D_z, R_{core}, and R_{batch} are adjusted numerically until the calculated fluxes Q_{g_St} and Q_{g_p} match the respective observed fluxes of 4 and 19 kg/s (Table 1). The value of T_{desc} was constrained in the range of 850–950 °C to ensure convergence.

Overall, our model considers seven free parameters (T_{desc}, Δh, D_z, ($z = 0$), $R_{z\ batch}$, R_{batch}^t, and R_{batch}^c or R_{core}) once all the other constraints are set. We considered in our analysis two values of Δh and 21 values of ($z = 0$), every pairing of which yields unique values for T_{desc}, D_z, R_{batch}^t, and R_{batch}^c/R_{core}. Since we use the output values of T_{desc} and R_{batch} to present our results, it is key to note that T_{desc} controls ρ_{desc} (Conflow) and μ_{desc} (Eq. (7)), which in turn directly affect batch radius through Eq. (15) because Q_{g_St} is constrained. The remaining parameter, $R_{z\ batch}$, is specific to spheroid batches and is under-constrained. A series of plausible values of $R_{z\ batch}$ is thus tested.

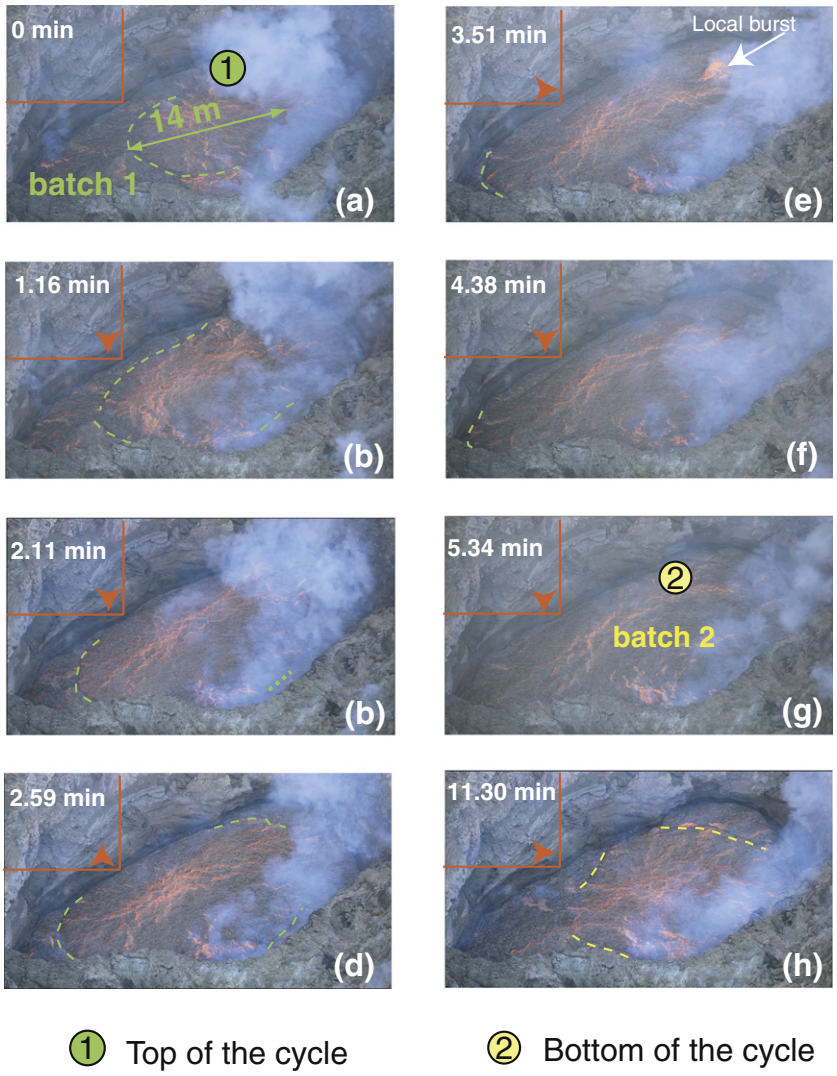

Fig. 4. Physical characteristics of the lava lake oscillations: (a) to (h) photographic sequence of lake oscillation associated to the arrival of two magma batches in December 20, 2010. Horizontal and vertical red lines form a reference position; the pointing direction of the red arrow indicates if the edge of the lake moves up, down, or remains still in relation with this reference. Values on the upper corner are times elapsed since image (a). Outlines are batches edges and labels 1 and 2 refer respectively to the high and low ends of the cycle.

3. Results

3.1. Field data

For convenience we compile published measurements of gas chemistry, temperature and flux from 2004–2005 (Fig. 1a; Oppenheimer et al., 2009; Peters et al., 2014b), along with infrared and photographic observations of the lake surface structure and elevation from December 2009 (Fig. 1b) and December 2010 (Fig. 4). The 2009 observations of Fig. 1b show a very similar pattern to the lake oscillations reported by Jones et al. (2015) and indicate a period of quiescence of 2 to 10 min, during which the lake level is low and stable, at the lowest of the gas flux cycle. A full cycle of oscillation lasts 22 to 30 min. This baseline height itself appears to fluctuate with a wavelength corresponding to a few hours though this is thought to be an artifact of the method of measuring the lake height (Fig. 1b).

Visual observations and measurements allow us to link the variations in gas composition and flux with the changes of velocity at the surface of the lake and the variation of its level, the former resulting from the inflation and deflation of the lake (Peters et al., 2014b). The lake level oscillations are on the order of 1 to 1.5 m amplitude with periods increasing by a factor of 2.2 to 3 between 2004 and 2009, while the area of the lake decreased by a factor of ~3 (Peters et al., 2014a). This suggests that the ascent rates of the magma flow causing the oscillations remain relatively constant. The 1–1.5 m amplitude surges in lake level therefore correspond to volume increases of order 770–1150 and 2500–3700 m^3 in 2004 and 2009, respectively. Averaged over the 10 and 20 min characteristic period of lake pulses, these correspond to mean volumetric rates of ~1–2 and ~2–3 $m^3\ s^{-1}$, respectively (Jones et al., 2015).

High resolution videos made in December, 2010 provide a detailed view of the arrival of consecutive batches of magma during the lava lake level fluctuation (Fig. 4). The duration of the films is limited to a maximum of 12 min. When speeded up (Movie 1 is available with the online version of the paper) they complement the information given by Oppenheimer et al. (2009).

The fluctuation of the level is not regular over the whole surface of the lake. The center of the lake swells, propagating a wave that spreads radially; reaching about 14 m in diameter (Fig. 4a). The wave is caused by the ascent of a gassy batch that reaches the surface and degasses. The degassed melt resulting from the previous batch sinks at the edge of the lake (Fig. 4b–c) as the magma of the current batch spreads and

overlaps the former (Fig. 4d); the level then seems to remain constant (Fig. 4d–e). The first wave of degassed magma reaches the edge of the lake after approximately ~5 min (Fig. 4f). This interval of 5 min corresponds exactly to the modal duration of half a cycle from 2004. Then the lake surface flattens until its center is lifted again by the arrival of a new gas-rich batch; it is therefore hotter, less viscous and less dense. Every batch disturbs the surface and results in its elevation with a rather similar pattern and sequence (Fig. 4g). Sometimes, a sudden and localized release of gas occurs (Fig. 4e) at different locations on the surface. There is a continuum between the small bubble bursting in Fig. 4e and large bubbles that rupture, ejecting lava bombs and evacuating part of the lake (e.g., Gerst et al., 2008).

The timescale for magma batch arrival is reasonably congruent with the appearance of concentric waves at the surface of the lake, which has a period of about ~5 min between consecutive batches or probably of ~10 min every other batch. We link the two consecutive waves to the ascent of batches of gas-rich magma of different composition that are in synchrony with the level change (i.e., the conduit gas composition causes the lowest flux in the cycle, and the top gas causes the highest flux). The image resolution could not allow us to appraise the size of the bubbles forming the batch with certainty. The cyclic radiative heat output observed by Oppenheimer et al. (2009) and the time difference between consecutive magma batches of different composition define the modal period of 10 min for a batch of identical composition (Fig. 4h) to reach surface from a specific location below surface and to be released. How those batches can be geochemically combined or intercalated and physically conceived will be explained in the next two sections, respectively.

3.2. Physical models

The synthesis of observations from December 2004 onwards indicates that the lake surface velocities are correlated with the changes in the chemical composition of the gases released at surface and that these changes also occur over cycles of 10 min. We thus set $T = 600$ s for scenarios 1 and 4 and $T = 300$ s for scenarios 2 and 3. Lake level changes in 2004 constrain Δh from 1 to 1.5 m, with a corresponding lake surface area, $S = 770$ m^2. To reduce the number of cases to consider, the impact of the larger surface area of the lake in 2004–2005 is assessed a posteriori with the most likely physical scenarios. Scenario likelihood is assessed using predicted conduit diameters. Observations of conduit diameter led us to group in three categories the possible outcome of the predicted conduit size at a depth of 20 m, which corresponds to the interface between lake and conduit. Runs are: (1) confirmed with "Yes" when $10 \geq R_{c\ max} > R_{batch}$ and $10 \geq R_{c\ min} > R_{batch}$, (2) accepted with "Perhaps" when $10 \leq R_{c\ max} > R_{batch}$ and $10 \geq R_{c\ min} > R_{batch}$ and (3) rejected when none of these criteria are met.

The remaining constraints come from the chemical modeling that quantifies the gas temperatures associated with the 2005 cycles. The chemical model by Burgisser et al. (2012) was used to obtain the melt water content, the average gas molecular weight, and the gas weight fraction as a function of pressure. The initial conditions were the three atmospheric gas compositions and surface porosities between 10 to 70 vol.% in steps of 10 vol.%, making a total of 21 runs in closed system (Table 1). Fig. 5 shows the evolution of total gas weight fraction with pressure for the three starting gases at three representative starting porosities. Overall, the amount of gas becomes negligible at pressures >100 MPa. As expected, the amount of exsolved volatiles decreases more abruptly with increasing pressure for the lake gas than for the top or conduit gases (Burgisser et al., 2012; Ilanko et al., 2015a). Fig. 5 shows an additional 3 runs assuming that the only volatile species is water and that it behaves ideally. These simplifications correspond to calculating W_{gT} as a function of P using Eq. (4) with the solubility law of the chemical model (i.e. melt H_2O content in wt.% is equal to $0.038 \times P^{0.677}$ with P in bars). The pure water runs severely underestimate the amount of gas in the magma batches because the volatile species are dominated by CO_2 at high pressure. As a result, the melt water content is over-estimated, which in turn leads to an underestimation of the batch viscosity and rising speed. The complexity introduced by the chemical model is necessary to accurately represent batch rise dynamics.

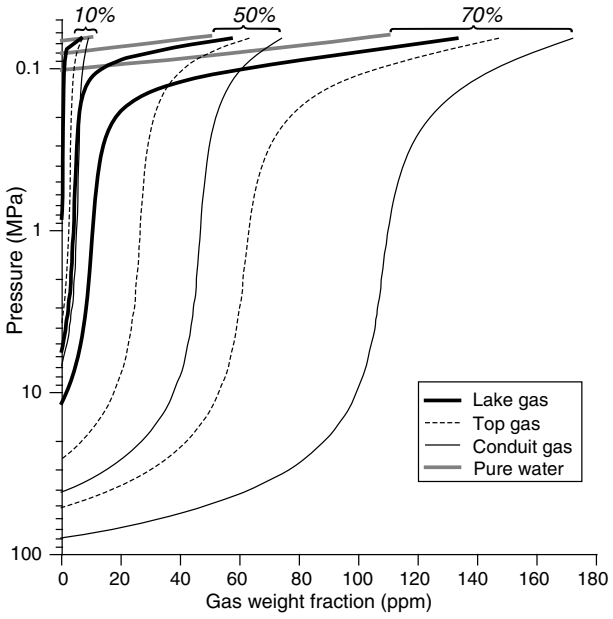

Fig. 5. Gas volume fraction as a function of pressure for representative closed-system runs of the chemical model of Burgisser et al. (2012). Initial compositions (labels lake gas, top gas, and conduit gas) and porosities (labels in italics indicating 10, 50, and 70 vol.%) at atmospheric pressure are taken from Table 1. Gray curves show runs assuming that the gas phase is pure water with the temperature and melt density of conduit gas.

The chemical runs were assembled in pairs according to the four physical scenarios to explain the oscillation amplitudes of either 1 or 1.5 m. Scenarios 1–3 used runs with the 7 increments in porosities and scenario 4 used runs with only two extreme initial porosities (10 and 70 vol.%, Table A1 with the online version of the paper), which yielded a total of 142 cases (Table A2 with the online version of the paper). The resulting ascent velocity values are in the order of 10^{-2} to 10^{-1} and 10^{-1} m/s for the low- and high-flux endmembers, respectively. This is consistent with their respective ascending temperatures, since the hotter magma batches are, the faster they ascend. Figs. 6–8 show the main results of the fitting procedure.

Initial porosities from the pairs of scenario 1, which involves spherical batches that match, for top-gas batches $T_{asc} = 1084$ °C, $Q_{gas} = 23$ kg/s, and $\Delta h = 1$ or 1.5 m, and for conduit-gas batches $T_{asc} = 1069$ °C and $Q_{gas} = 19$ kg/s are shown in Fig. 6A (cases 1–26 of Tables A1–A2 with the online version of the paper). Fig. 6B–C shows six model outputs as a function of T_{desc} that are compared with the independent observation that the conduit radius is 10 ± 5 m. These outputs, maximum and minimum conduit radius and batch radius for each batch type, were estimated at 20 m depth, which represents the top of the conduit. Two pairs (cases 9–10 and 15–16) were eliminated from further analysis because their ascent speeds (i.e., $<10^{-4}$ m/s) are so slow that they rise by less than a batch diameter in 10 min.

It is apparent in Fig. 6 that fixing the surface porosity of the conduit-gas batch at 70 vol.% yields the smallest radii at 20 m depth and the smallest upper and lower bounds of conduit radius. Keeping the conduit-gas batch porosity at 70%, it is when the top-gas batch porosity is highest (70%) that all conduit radii estimates yield similar values, from 10 m for the minimum radius to 16–18 m for the maximum radius, regardless of Δh and batch type. When the top-gas batch porosity is low (20 vol.% minimum), conduit radius estimates based on the top-gas batch are much higher (13–30 m for 20 vol.%) than those based on the

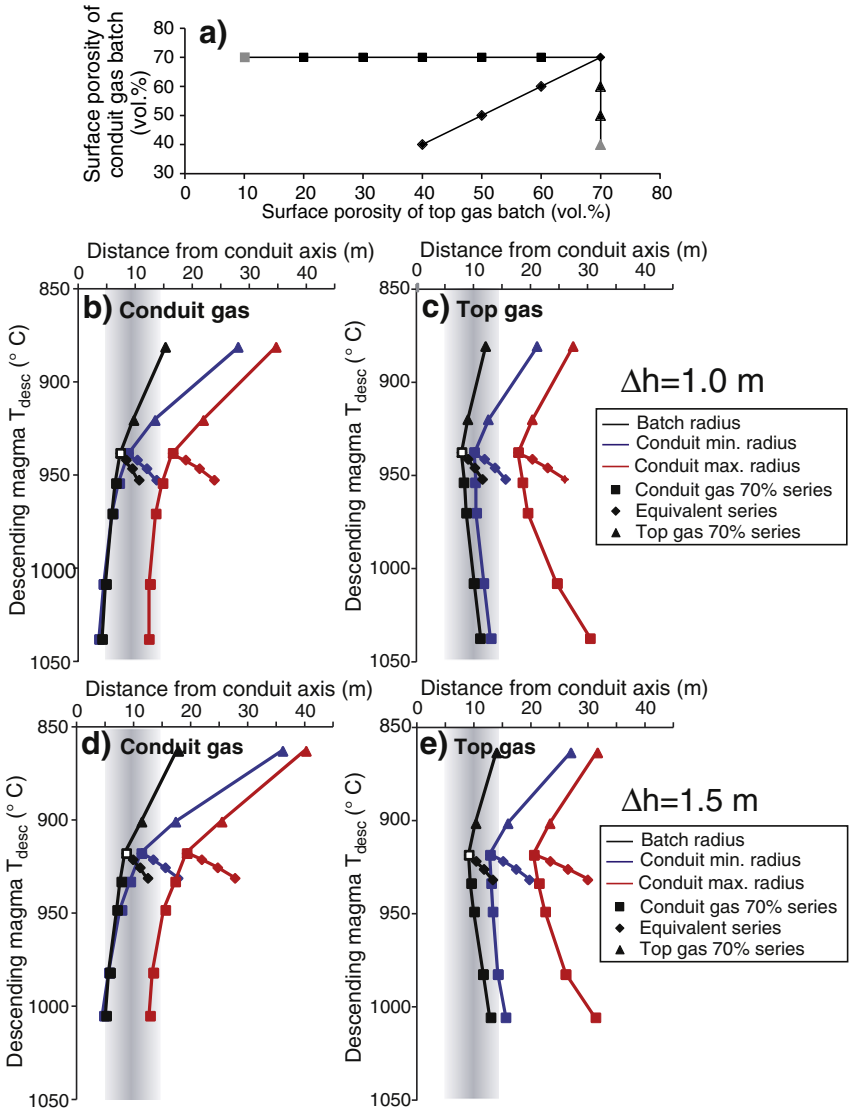

Fig. 6. Results from scenario 1 involving spherical batches that match, for top-gas batches T_{asc} = 1084 °C, Q_{gas} = 23 kg/s and Δh = 1 m or 1.5 m, and for conduit-gas batches T_{asc} = 1069 °C and Q_{gas} = 19 kg/s: (A) Three series of cases that each pair a top-gas spherical batch with given surface porosity and a conduit-gas batch of another given porosity. Squares mark cases with a constant conduit-gas batch porosity of 70 vol.%, diamonds mark cases with both batch types of equal porosities and triangles marks cases with a constant top-gas batch porosity of 70 vol.%. The two gray symbols indicate cases (9/10 and 15/16) with batch ascent speeds so slow that they would rise by less than a batch diameter in 10 min. These cases were discarded in (B)–(C)–(D). (B)–(C) Distance from conduit axis at 20 m depth as a function of descending magma temperature for Δh = 1 m. (D)–(E) Distance from conduit axis at 20 m depth as a function of descending magma temperature for Δh = 1.5 m. Black values are batch radii, blue values are minimum conduit radii (Eq. (14b)) and red values are maximum conduit radii (Eq. (14a)). The gray vertical area indicates the likely conduit radius at Erebus from independent observations. Surface porosities of each case can be found by referencing the case of interest to the case with 70 vol.% porosities for both top-gas and conduit-gas batches (open square) in (A).

conduit-gas batch (4–12 m for 20 vol.%). These considerations and the independent evidence that the probable conduit radius at Erebus is closer to 5 m than to 15 m make the pairs with conduit-gas batch porosities of 70 vol.% and top-gas batch porosities ranging from 20 to 70 vol.% the most likely candidates for scenario 1. As a result, likely descending magma temperatures range from ~940 to ~1040 °C.

Results from scenario 1 suggest that the smallest conduit radius estimates are between 8.5 and 10 m, which is still high. Scenario 4 assumes that batches are constricted by a narrow conduit. When calculating the spheroid evolution with increasing depth, smaller and smaller batch volumes are found because of the increasing pressure reduces vesicularity. Since the horizontal radius of the spheroid is fixed, there may be a level below which the vertical axis of the spheroid becomes shorter than the horizontal one. This is an unlikely configuration for a rising batch and so our model calculates instead a spherical radius by applying mass conservation. The conduit starts around 20 m depth, and it is unlikely that the switch between spheroid and sphere occurs in the lake because of the wide shape of the lake floor. We thus added the constraint that the switch spheroid/sphere has to occur deeper than 20 m to retain the solution. Another modified constraint is the detachment depth, which is redefined such that batch ascent speeds should be fast enough for a batch to rise a distance greater than the batch vertical extension in 10 min. Other constraints are to the same as those for scenario 1.

Spheroids have two independent radii, which introduces an unconstrained degree of freedom compared to spherical batches. To frame the possible parameter ranges while limiting the number of cases to consider, we only calculated two pairs of surface porosities (70–10 vol.% and 70–70 vol.%). The horizontal radius of the batch with conduit gas composition was fixed at three possible values (2, 4 and 6 m) and the one with top gas composition was fixed at representative values in regular increments. Each combination was run with a Δh of either 1 or 1.5 m, yielding 64 cases (Table A2 with the online version of the paper).

Fig. 7 shows the solutions of possible spheroidal batch pairs that correspond to cases 79–142 (Tables A1–A2 with the online version of the paper). The solutions are grouped in curves for different fixed conduit-gas batch horizontal radius and by batch types (upwards arrows for top-gas batches and downwards arrows for conduit-gas batches). Curves mark the distance from the conduit axis at 20 m depth as a function of descending magma temperature. When Δh = 1 m, curves with temperature above 950 °C correspond to a conduit-gas batch of 70 vol.% surface porosity paired with a top-gas batch of 10 vol.% surface porosity (Fig. 7a). Increasing Δh to 1.5 m shifts these curves towards lower temperature by ~100 °C (Fig. 7b). On the other hand, curves below 950 °C when Δh = 1 m correspond to top- and conduit-gas batches surface porosities of 70 vol.%. They have smaller radii values than curves >950 °C and increasing Δh to 1.5 m causes a smaller (~50 °C) shift towards lower temperature (Fig. 7b).

Scenarios 2 and 3 assume that the high-end of the flux cycle reflects a mixture between the conduit gas and the lake gas. If the conduit gas is carried by discrete batches, scenario 2 indicates that no solutions matching the required constraints can be found for the batches carrying the conduit gas (cases 27–52, Tables A1–A2 with the online version of the paper). If the conduit gas is carried instead by a continuous flow, scenario 3 indicates that the radius of the batches carrying the lake gas is systematically too large (>10 m) if the batches have a 70 vol.% surface porosity (cases 66–78, Tables A1–A2 with the online version of the paper). Lower surface porosities for the lake gas batches yield smaller flow radii but no pairs satisfy all conduit size criteria (cases 53–65, Tables A1–A2 with the online version of the paper). Since most of the lake gas batches originate at shallow depths (100–500 m) and have detachment depths <20 m, our results point to a possible flow dynamics restricted to the lava lake, where conduit radius constraints no longer apply. Lake-gas batch sizes are such (10–16 m in equivalent diameter) that they would fill up a substantial part of the lake. They would not rise as discrete spheres but cause an overturn motion within the lake, which no longer fits the setup of scenario 3. Our results thus suggest that scenarios 2 and 3 cannot be reconciled with the observations and are therefore rejected.

There are two scenarios (1 and 4) among the four tested that contain cases that satisfy all constraints. The *Re* values of these cases (bold font in Table A3) lie between 10^{-3} and 10^{-2}, well below the maximum limit of our model (Re = 5). Most successful cases belong to scenario 4 (79–82, 84–86, 89–93, 98–99, 107, and 114) while only case 7 belongs to scenario 1. The fluctuation of the lava lake level is more likely to be caused by batches that are constricted by the narrow size of the conduit in the last part of their upwards journey. All the other cases were rejected because either it was not possible to fit the observed gas fluxes (e.g., case 10, Table A2 with the online version of the paper), or one batch type rises by less that its diameter in 10 min above the "generation depth" (e.g. case 9, Table A2 with the online version of the paper), or the batch and/or conduit size estimates exceeded the inferred conduit size (e.g. cases 27–52, Table A2 with the online version of the paper). We use cases 7, 79 and 107 as representative and depict their geometrical evolution as a function of depth and time in Fig. 8.

Average extreme values of conduit diameters of these cases suggest that batches can be fitted in a conduit of 12 to 24 m in diameter, respectively. Overall, our results suggest that a water-rich gas (73 mol%) and hot (1085 °C) buoyant magma with a composition of "top gas" could vesiculate as deep as ~2000 m. As the magma rises in the conduit, the pressure drop leads to a sharp acceleration as it nears the surface to reach 70 vol.% porosity (Fig. 8). Individual batches detach from the rising magma at different depths; most of the accepted cases from scenario 4 (e.g., Fig. 8b–8c) indicate depth values between 50–100 m while the only case from scenario 1 (Fig. 8a) shows a deeper value (~250 m). From a minimum depth of ~30 m they reach the surface every 10 min to release 23 kg/s of gas (Fig. 8). They alternate with batches with a composition of "conduit gas", which are slower, colder (1069 °C), less water-rich (60 mol%). Those batches could have originated in the deeper part of the system (~3000 m deep). These colder batches detach also around 20–100 m (if scenario 4) or deeper (200 m if scenario 1) and accelerate at a depth of ~30 m to reach the lake surface every 10 min with a porosity of 70 vol.% and release 19 kg/s of gas to the atmosphere (Fig. 8). The temperature of the descending flow is between 890 and 950 °C, which is roughly 100 °C colder than the ascending currents.

Batches initiate deep below the surface and their ascent lasts more than the timespan separating two degassing events (see Table A3 with the online version of the paper) between the lake floor and the

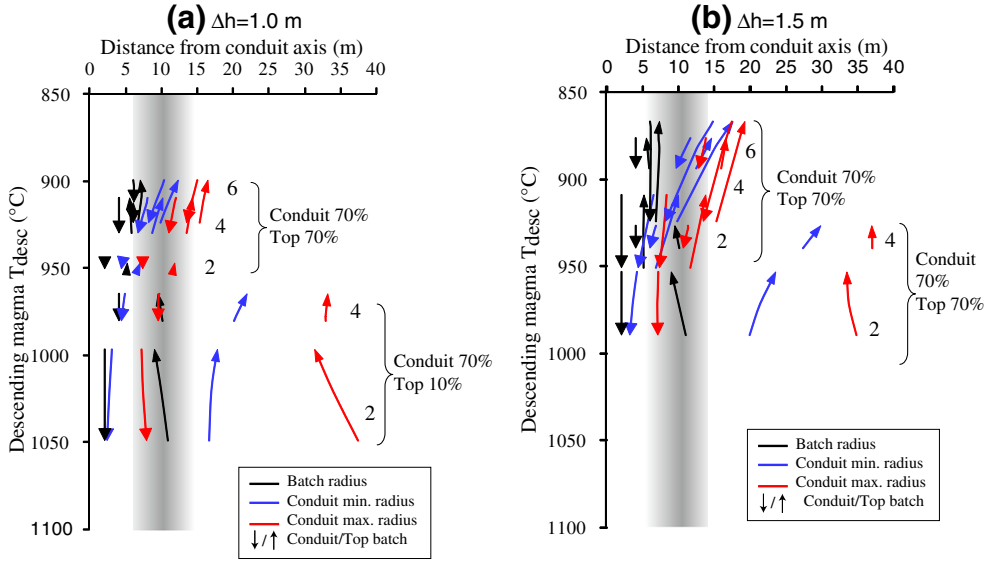

Fig. 7. Results from scenarios involving spheroidal batches that match, for top-gas batches T_{asc} = 1084 °C, Q_{gas} = 23 kg/s and Δh = 1 m or 1.5 m, and for conduit-gas batches T_{asc} = 1069 °C and Q_{gas} = 19 kg/s: (a) Distance from conduit axis at 20 m depth as a function of descending magma temperature for Δh = 1.0 m. (b) Distance from conduit axis at 20 m depth as a function of descending magma temperature for Δh = 1.5 m. Black curves are batch radii, blue curves are minimum conduit radii (Eq. (14b)) and red curves are maximum conduit radii (Eq. (14a)). The gray vertical area indicates the likely conduit radius at Erebus from independent observations. Bold labels (2, 4, and 6) are fixed horizontal radii at the surface for the conduit-gas batches, which each characterize a series of three upward pointing arrows (top-gas batches) and three downward pointing arrows (conduit-gas batches). Labels next to curly braces indicate surface porosities of each series of pairs.

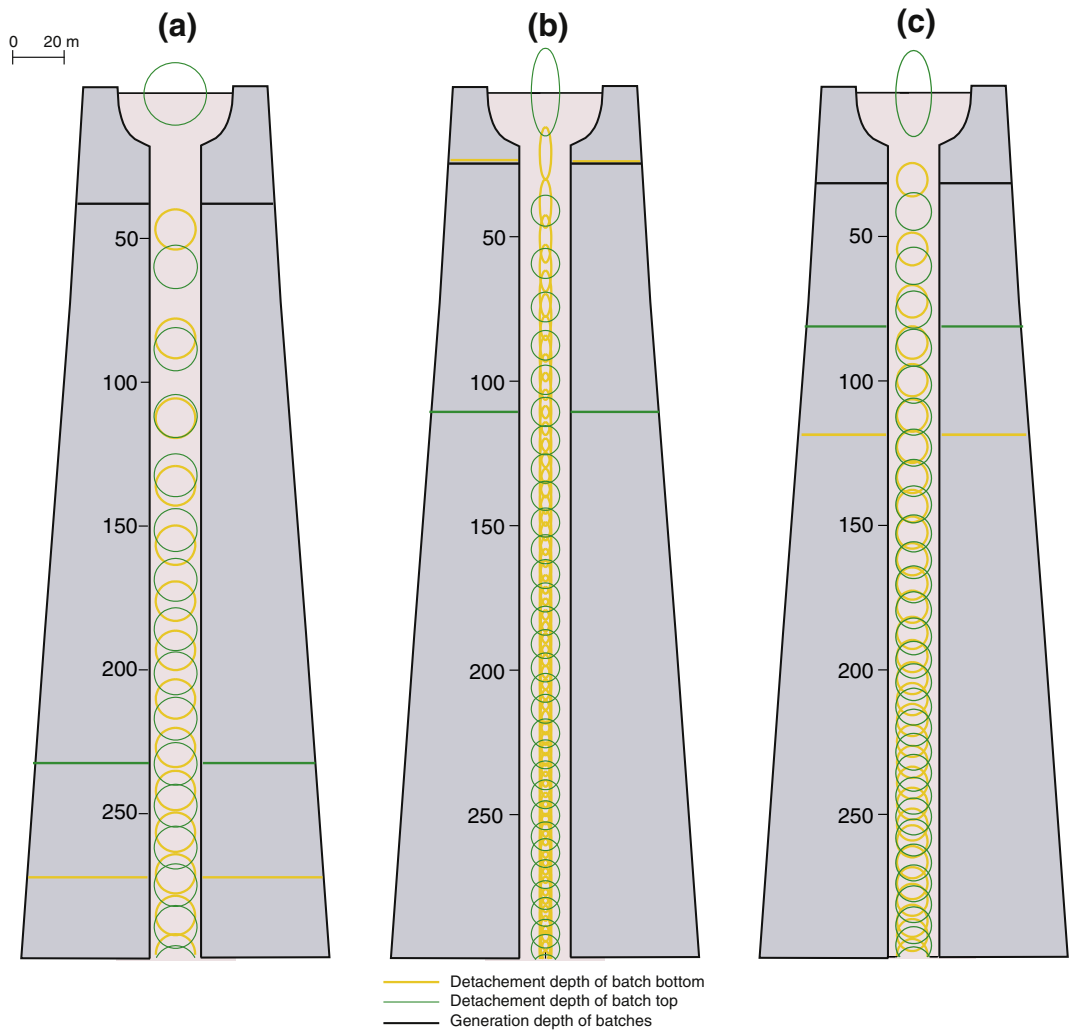

Fig. 8. Illustration of three possible scenarios to explain the oscillations of Erebus lava lake as a function of depth (m). (a) Alternating spherical batches of conduit (yellow) and top (green) gas compositions (Case 7 of scenario 1; Table A2 with the online version of the paper). (b) Alternating spheroidal batches of conduit (yellow) and top (green) gas compositions (Case 79 of scenario 4; Table A2 with the online version of the paper). (c) Alternating spheroidal batches of conduit (yellow) and top (green) gas compositions (Case 107 of scenario 4; Table A2 with the online version of the paper).

generation depth. Therefore, new batches are already rising in sequence when a batch is released at the surface and they are not initiated by the pressure drop caused by degassing and the change in level of the lake.

Our results suggest that matching the gas flux oscillations with a lake level change of 1–1.5 m requires a temperature difference between ascending and descending magma of 115–195 °C (the higher value corresponding to top gas composition and conversely) with spherical batches, or batches evolving from spherical to spheroidal geometries, reaching 70 vol.% surface porosity. Those batches would have ~4 m and 14 m diameter at the surface, respectively (see Table A1 with the online version of the paper). This range of diameter coincides with our observations of video data that the batch arriving at surface generates a surging disturbance of ~14 m diameter (Fig. 4a).

If gas fluxes of 19 and 23 kg/s are representative of the period of observations in 2009, when the lake surface area was 2500 m^2, with a mean period of 20 min and 1-m oscillation, then the corresponding temperature difference would have been 184 °C and 199 °C for spherical batches of conduit- and top-gas compositions, respectively; the diameter of those batches would be ~29 m and 32 m in the conduit and at surface, respectively. However, this scenario is not consistent with our criteria, because the batch itself would be larger than the acceptable conduit diameter. If we consider instead a constrained, spheroidal batch of 2-m horizontal radius like case 79 (Table A2 with the online version of the paper), the temperature difference would have been of 105 °C and 120 °C for spheroids of conduit- and top-gas compositions, respectively; those batches would be ~4 and 10 m in diameter in the conduit and at the surface, respectively. This estimate suggests that our results, which are mostly based on 2004–2005 field data, are not sensitive to observed changes in lake surface area and/or oscillation period over the past decade.

4. Discussion

Visual observations and outputs from our physical models of magma circulation lead us to interpret the general dynamics of the lava lake rise and fall as follows. At depth, the magma containing dissolved gas rises by buoyancy. As pressure decreases, the gas exsolving from the melt causes the ascent velocity to increase. When the upward flow reaches the detachment depth, it behaves as differentiated batches, the velocity of which increases. The cause of batch generation is not explicitly addressed in our model and is assumed to reflect flow instability. When a given batch reaches the surface, the level of the lake increases under the extra supply of bubbly magma and the batch releases its gas to atmosphere while the degassed melt is spreading towards the edges of the lava lake. The degassing rate decreases and the melt keeps spreading laterally as the whole surface tends to flatten; the “fresh” melt overlaps

the cooler and harder surface formed by the previous batches of magma. The process is cyclical because other batches having formed at the detachment depth are already on their way to the surface, which they reach periodically. The denser, colder, and degassed magma is drained back in the conduit and down to the magma chamber as lighter bubbly magma travels upwards in the same conduit.

The four scenarios we analyzed are differentiated by the type of ascending flux (Poiseuille/batch), the gas composition ("lake gas", "conduit gas", and "top gas") and the associated gas flux (4, 19 or 23 kg/s, respectively). No solutions could be found when the high end of the flux cycle is made of a mixture of conduit gas and lake gas, regardless of whether the conduit gas is carried by discrete batches, or by steady-state Poiseuille flow (scenarios 2–3). This suggests that the compositional cycles reflect two distinct chemical signatures that do not mix and that originate from deeper than the lake (scenarios 1 and 4). These poles correspond to magma batch pairs that have shapes likely constrained by the conduit width because more cases are valid for scenario 4 than scenario 1. Regardless of their shapes, the pairs reach very high porosities near the surface (70 vol.%) compatible with our assumed physical template of a bubbly magma. The tight alternating arrival of these large (~14 m in diameter) batches brings forth the image of a lava lake mostly filled with gas-rich magma. Since high porosity is often associated with the development of a permeable network of gas bubbles, this is consistent with the high gas permeability of the lake inferred from observations (Peters et al., 2014a) and gas flux measurements (Peters et al., 2014b).

The conduit geometry we adopted is highly simplified. Further findings about the width and geometry of the conduit would change our results by accepting more scenarios if the conduit is wider than thought. On the contrary, a significantly smaller conduit, say 5 m in diameter (Ilanko et al., 2015b), would render most of our cases unlikely. This latter case would point to flow instabilities that are incipient and do not lead to discrete magma batches. Another limitation is the requirement that batch types do not mix while rising. If instead the medium is considered as a continuum, batches of different sizes and compositions (e.g., discarded cases from scenarios 2–4) could coexist and alter each other's properties (i.e., velocity, porosities, compositions), resulting in hybrid batches or conduit-wide mixing (Palma et al., 2011). The physical template we used herein cannot accommodate such complexities, which call for a different approach. We thus see our approach as providing the first-order conclusion that instability of the bidirectional flow in the shallow Erebus magmatic system is a viable physical mechanism to explain oscillations of the lava lake.

Phonolite lava temperatures derived from petrological evidence span from 925 to 1030 °C (Kyle, 1977; Dunbar et al., 1994; Moussallam et al., 2013). Gas modeling indicates yearly variations from 1000 to 1085 °C (Burgisser et al., 2012; Moussallam et al., 2013; Alletti et al., 2014). Our results suggest that the temperature difference between up- and downflows is between 100–200 °C, which is close to the 200 °C proposed by Calkins et al. (2008) to explain the minimum mass supply rate of the lake. Gathering the various temperature estimates of the active magmatic system at Erebus points to a shallow part dominated by colder descending magma around 900–950 °C fed by a deeper, warmer system around 1000–1050 °C. Precise localization of the deeper, hotter source is difficult. Our results suggest that batch dynamics are restricted to the upper 250 m of the conduit while the generation depth of the upward flow is 2–3 km, assuming closed-system degassing (see also Burgisser et al., 2012; Alletti et al., 2014). These depths point to an active convective system reaching a few kilometers below the lake, which is agreement with the trajectories of single anorthoclase crystals tracked by Moussallam et al. (2015) that suggest rapid magma transfers in the upper few kilometers of the magmatic system.

The picture of a magma system stirred in its upper few kilometers is consistent with batches rising from a single phonolitic magma that reach the surface with a differentiated volatile composition. The reason behind this differentiation is not a difference in bubble growth rate (Burgisser et al., 2012). Chemical modeling alone, however, does not provide volatile evolutions as a function of pressure that are precise enough to indicate an unequivocal cause of differentiation. Assuming constant temperature in the rising magma, such modeling simply suggests that the greatest potential for differentiation occurs in the last hundred meters of the magma ascent as a result of degassing style (open vs. closed system) (Burgisser et al., 2012; Alletti et al., 2014). Considering our results, the chemical effects of the 100–200 °C temperature variations caused by the mixing of descending magma in the warmer resident magma reservoir might explain the differentiation. Should this process be dominant, it opens the possibility that the chemical cycles observed are a natural consequence of the convective motion and the associated temperature contrasts. In this view, the descending magma is likely to be reheated as it reaches the magmatic reservoir, depleting it in volatiles by dilution. The overpressure driving this permanent degassing is mainly due to the buoyancy between the gas-rich rising magma and the denser degassed magma, without additional injection of gas and magma in the reservoir. We expect that the importance of such a closed-system convective degassing is controlled by the volume ratio between resident and descending magma, which bears on the unresolved issue of the size of the magmatic reservoir beneath Erebus (Moussallam et al., 2014).

5. Conclusions

We used a simple fluid dynamical model to explain the cyclic behavior of the lava lake at Erebus. By setting constraints such as the magma volume causing the lava lake oscillation, the measured chemistry and fluxes of the emitted gases, and the geometry of the lake and conduit, we explored four scenarios for the ascent of magma batches with distinct gas compositions. Each scenario has a subset of model runs that involve magma batch pairs with varying characteristics. Solutions for the 142 cases tested in total were found by adjusting the temperature of the descending magma and the baseline height of the lake. Their consistency was tested by comparing the resulting conduit diameter with independent observations.

Our results suggest that the high end of the flux cycles, when the lava lake is at its highest, is not the result of the mixing of a magma source originating from the lake with a deeper source. It is instead caused by a discrete source of water-rich (73 mol%) and hot (1085 °C) buoyant magma that vesiculates as deep as ~2000 m. As the magma rises in the conduit, the pressure to which it is submitted decreases and leads to a progressive acceleration. Individual batches detach from the rising magma at depths of 50–250 m. The low end of the flux cycles is the result of a discrete pole of colder (1069 °C) and less water-rich (60 mol%) magma. This colder magma could vesiculate deeper (~3000 m) than its hot counterpart. Individual batches detach also around 20–200 m deep. The two batch types can coexist in a single conduit up to a depth of ~30 m, above which they rise alternatively to release respectively 19 and 23 kg/s of gas at the lake surface every 10 min. The temperature of the descending flow is between 890 and 950 °C, which is roughly 100 °C colder than the ascending currents. Batch pairs have shapes likely constrained by the conduit width. Regardless of their shapes, the pairs reach very high porosities near the surface and have diameters of 4–14 m that are consistent with video observations showing spreading waves at the lake surface. The tight alternative arrival of these large batches brings forth the image of a lava lake mostly filled with gas-rich magma.

Supplementary data to this article can be found online at http://dx.doi.org/10.1016/j.jvolgeores.2015.10.027.

Acknowledgments

This work is part of the first author's PhD thesis, which was funded by the 7th Framework Program of the EC (ERC grant 202844) and by Senescyt under the Prometeo Program (Ecuador). CO acknowledges

support from the Isaac Newton Trust (project "Physical constraints for the interpretation of open-vent volcanism") and the Natural Environment Research Council (National Centre for Earth Observation: COMET). We greatly appreciate the thorough review and detailed comments from P-Y Burgi that helped us to improve the understanding of the initial version of the manuscript.

Appendix A

We calculated the velocity of any ascending batch, U_{batch}, by solving the polynomial of second order after re-arranging Eqs. (8) and (9):

$$\frac{3}{8}\frac{R_{batch}\rho_{desc}}{\alpha+\beta}\,M\,U_{batch}^2+\frac{\mu_{desc}}{\alpha+\beta}M\,U_{batch}-\frac{1}{4}g\,R_{z\,batch}R_{batch}^2(\rho_{desc}-_{batch})=0 \tag{A1}$$

in which $M=\frac{2\mu_{desc}+3\mu_{asc}}{\mu_{desc}+\mu_{asc}}$.

The positive solution of that polynomial is given by:

$$U_{batch}(z)=\frac{4}{3}\frac{\sqrt{(\mu_{desc}M)^2+\frac{3}{8}\rho_{desc}R_{z\,batch}R_{batch}^3(\rho_{desc}-\rho_{batch})Mg(\alpha+\beta)}-\mu_{desc}M}{R_{batch}\rho_{desc}M} \tag{A2}$$

where α and β are the geometrical factors defined by McNown and Malaika (1950) for a prolate spheroid (their case 4):

$$\alpha=\frac{2}{\sqrt{R_{z\,batch}^2-R_{batch}^2}}\tanh^{-1}\frac{\sqrt{R_{z\,batch}^2-R_{batch}^2}}{R_{batch}}$$

$$\beta=\frac{2R_{z\,batch}^2}{\sqrt{\left(R_{z\,batch}^2-R_{batch}^2\right)^3}}\left(\tanh^{-1}\frac{\sqrt{R_{z\,batch}^2-R_{batch}^2}}{R_{batch}}-\frac{\sqrt{R_{z\,batch}^2-R_{batch}^2}}{R_{batch}}\right) \tag{A3a}$$

and for spherical geometries (their case 1):

$$\alpha=2/R_{z\,batch}$$
$$\beta=2/3\,R_{z\,batch} \tag{A3b}$$

Once we know the velocity of the batch as a function of depth, we can calculate the rise time. At the instant t_{i-1} the velocity of the batch is $U_{batch_{i-1}}$, at the instant t_i the velocity of the batch is U_{batch_i}. The average velocity U_{batch} in the time interval $\Delta t_i = t_i - t_{i-1}$ is $U_{batch} = [U_{batch}(z_i) + U_{batch}(z_{i-1})]/2$ and the time for a batch to ascend from z_{i-1} to z_i is approximated by:

$$t_i\approx\frac{z_i-z_{i-1}}{U_{batch}}+t_{i-1} \tag{A4}$$

References

Alletti, M., Burgisser, A., Scaillet, B., Oppenheimer, C., 2014. Chloride partitioning and solubility in hydrous phonolites from Erebus volcano: A contribution towards a multi-component degassing model. GeoResJ 3–4, 27–45.

Aster, R., Mah, S., Kyle, P., McIntosh, W., Dunbar, N., Johnson, J., Ruiz, M., McNamara, S., 2003. Very long period oscillations of Mount Erebus volcano. J. Geophys. Res. 108 (B11), 2522. http://dx.doi.org/10.1029/2002JB002101.

Beckett, F.M., Burton, M., Mader, H.M., Phillips, J.C., Polacci, M., Rust, A.C., Witham, F., 2014. Conduit convection driving persistent degassing at basaltic volcanoes. J. Volcanol. Geotherm. Res. 283, 19–35.

Boichu, M., Oppenheimmer, C., Tsanev, V., Kyle, P.R., 2010. High temporal resolution SO_2 flux measurements at Erebus volcano. J. Volcanol. Geotherm. Res. 190 (3–4), 325–336.

Burgisser, A., Scaillet, Harshvardhan, B., 2008. Chemical patterns of erupting silicic magmas and their influence on the amount of degassing during ascent. J. Geophys. Res. 113, B12204. http://dx.doi.org/10.1029/2008JB005680.

Burgisser, A., Oppenheimer, C., Alletti, M., Kyle, P.R., Scaillet, B., Carrol, M., 2012. Backward tracking of gas chemistry measurements at Erebus volcano. Geochem. Geophys. Geosyst. 13 (11). http://dx.doi.org/10.1029/2012GC004243.

Burgisser, A., Alletti, M., Scaillet, B., 2015. Simulating the behavior of volatiles belonging to the C–O–H–S system in silicate melts under magmatic conditions with the software D-Compress. Comput. Geosci. 79, 1–14.

Calkins, J., Oppenheimer, C., Kyle, P.R., 2008. Ground-based thermal imaging of lava lakes at Erebus volcano, Antarctica. J. Volcanol. Geotherm. Res. 177, 695–704.

Crowe, C., Sommerfeld, M., Tsuji, Y.H., 1997. Multiphase flows with droplets and particles. CRC Press.

Dibble, R.R., Kyle, P.R., Rowe, C.A., 2008. Video and seismic observations of Strombolian eruptions at Erebus volcano, Antarctica. J. Volcanol. Geotherm. Res. 177, 619–634. http://dx.doi.org/10.1016/j.jvolgeores.2008.07.020.

Dunbar, N.W., Cashman, K.V., Dupré, R., 1994. Crystallization processes of anorthoclase phenocrysts in the Mount Erebus magmatic system: evidence from crystal composition, crystal size distributions, and volatile contents of melt inclusions. In: Kyle, P.R. (Ed.), Volcanological and environmental studies of Mount Erebus, Antarctica, Antarctic Research Series. Amer. Geophys. U 66, pp. 129–146.

Gerst, A., Hort, M., Kyle, P.R., 2008. 4D velocity of Strombolian eruptions and man-made explosions derived from multiple Doppler radar instruments. J. Volcanol. Geotherm. Res. 177 (3), 648–660. http://dx.doi.org/10.1016/j.jvolgeores.2008.05.022.

Giordano, D., Russell, J.K., Dingwell, D.B., 2008. Viscosity of magmatic liquids: a model. Earth Planet. Sci. Lett. 271, 123–134. http://dx.doi.org/10.1016/j.epsl.2008.03.038.

Ilanko, T., Oppenheimer, C., Burgisser, A., Kyle, P.R., 2015a. Cyclic degassing of Erebus volcano, Antarctica. Bull. Volcanol. 77, 56. http://dx.doi.org/10.1007/s00445-015-0941-z.

Ilanko, T., Oppenheimer, C., Burgisser, A., Kyle, P.R., 2015b. Transient degassing events at the lava lake of Erebus volcano, Antarctica: chemistry and mechanisms. GeoResJ 7, 43–58.

Jones, L.K., Kyle, P.R., Oppenheimer, C., Frechette, J.D., Okal, M.H., 2015. Terrestrial laser scanning observations of geomorphic changes and varying lava lake levels at Erebus volcano, Antarctica. J. Volcanol. Geotherm. Res. 295, 43–54.

Kazahaya, K., Shinohara, H., Saito, G., 1994. Excessive degassing of Izu-Oshima volcano: magma convection in a conduit. Bull. Volcanol. 56, 207–216.

Kelly, P.J., Kyle, P.R., Dunbar, N.W., Sims, K.W.W., 2008. Geochemistry and mineralogy of the phonolite lava lake, Erebus volcano, Antarctica: 1972–2004 and comparison with older lavas. J. Volcanol. Geotherm. Res. 177, 589–605. http://dx.doi.org/10.1016/j.jvolgeores.2007.11.025.

Koyaguchi, T., 1985. Magma mixing in a conduit. J. Volcanol. Geotherm. Res. 25, 365–369.

Krieger, I.M., Dougherty, T.J., 1959. A mechanism for non-Newtonian flow in suspensions of rigid spheres. Trans. Soc. Rheol. 3, 137–152.

Kyle, P.R., 1977. Mineralogy and glass chemistry of recent volcanic ejecta from Mt Erebus, Ross Island, Antarctica. N. Z. J. Geol. Geophys. 20, 1123–1146.

Lamb, H., 1945. Hydrodynamics. Cambridge University Press, Cambridge (738 pp.).

Le Losq, C., Neuville, D.R., Moretti, R., Kyle, P.R., Oppenheimer, C., 2015. Rheology of phonolitic magmas — the case of the Erebus lava lake. Earth Planet. Sci. Lett. 411, 53–61.

Mastin, L., Ghiorso, M., 2000. A numerical program for steady-state flow of magma-gas mixtures through vertical eruptive conduits. Open-File Report of the USGS, pp. 1–53.

McClelland, L., Simkin, T., Summers, M., Nielsen, E., Stein, T.C., 1989. Global volcanism 1975–1985. Prentice Hall, New Jersey.

McNown, J.S., Malaika, J., 1950. Effects of particle shape on settling velocity at low Reynolds numbers. Eos. Trans. AGU 31 (1), 74–82. http://dx.doi.org/10.1029/TR031i001p00074.

Molina, I., Burgisser, A., Oppenheimer, C., 2012. Numerical simulations of convection in crystal-bearing magmas: a case study of the magmatic system at Erebus, Antarctica. J. Geophys. Res. 117, B07209. http://dx.doi.org/10.1029/2011JB008760.

Moussallam, Y., Oppenheimer, C., Scaillet, B., Kyle, P.R., 2013. Experimental phase-equilibrium constraints on the phonolite magmatic system of Erebus volcano, Antarctica. J. Petrol. 54, 1285–1307.

Moussallam, Y., Oppenheimer, C., Scaillet, B., Gaillard, F., Kyle, P., Peters, N., Hartley, M., Berlo, K., Donovan, A., 2014. Tracking the changing oxidation state of Erebus magmas, from mantle to surface, driven by magma ascent and degassing. Earth Planet. Sci. Lett. 393, 200–209.

Moussallam, Y., Oppenheimer, C., Scaillet, B., Buisman, I., Kimball, C., Dunbar, N., Burgisser, A., Schipper, C.I., Andújar, J., Kyle, P.R., 2015. Megacrystals track magma convection between reservoir and surface. Earth Planet. Sci. Lett. 413, 1–12.

Oppenheimer, C., Lomakina, A.S., Kyle, P.R., Kingsbury, N.G., Boichu, M., 2009. Pulsatory magma supply to a phonolite lava lake. Earth Planet. Sci. Lett. 284, 392–398.

Palma, J.L., Blake, S., Calder, E.S., 2011. Constraints on the rates of degassing and convection in basaltic open-vent volcanoes. Geochem. Geophys. Geosyst. 12, Q11006. http://dx.doi.org/10.1029/2011GC003715.

Patrick, M.R., Orr, T., Antolik, L., Lee, L., Kamibayashi, K., 2014. Continuous monitoring of Hawaiian volcanoes with thermal cameras. J. Appl. Volcanol. 3 (1), 1–19.

Peters, N., Oppenheimer, C., Kyle, P., Kingsbury, N., 2014a. Decadal persistence of cycles in lava lake motion at Erebus volcano, Antarctica. Earth Planet. Sci. Lett. 395, 1–12. http://dx.doi.org/10.1016/j.epsl.2014.03.032.

Peters, N., Oppenheimer, C., Killingsworth, D.R., Frechette, J., Kyle, P., 2014b. Correlation of cycles in lava lake motion and degassing at Erebus volcano, Antarctica. Geochem. Geophys. Geosyst. 15, 3244–3257. http://dx.doi.org/10.1002/2014GC005399.

Petford, N., 2009. Which effective viscosity? Mineral. Mag. 73 (2), 167–191. http://dx.doi.org/10.1180/minmag.2009.073.2.167.

Shimozuru, C., 1978. Dynamics of magma in a volcanic conduit — special emphasis on viscosity of magma with bubbles. Bull. Volcanol. 41 (4), 333–340.

Stevenson, D.S., Blake, S., 1998. Modeling the dynamics and thermodynamics of volcanic degassing. Bull. Volcanol. 60, 307–317.

Sweeney, D., Kyle, P.R., Oppenheimer, C., 2008. Sulfur dioxide emissions and degassing behavior of Erebus volcano, Antarctica. J. Volcanol. Geotherm. Res. 177, 725–733. http://dx.doi.org/10.1016/j.jvolgeores.2008.01.024.

Weinberg, R.F., Podladchikov, Y., 1994. Diapiric ascent of magmas through power law crust and mantle. J. Geophys. Res. 99 (B5), 9543–9559. http://dx.doi.org/10.1029/93JB03461.

Witham, F., Llewellin, E.W., 2006. Stability of lava lakes. J. Volcanol. Geotherm. Res. 158, 321–332.

Witham, F., Woods, A.W., Gladstone, C., 2006. An analogue experiment model of depth fluctuations in lava lakes. Bull. Volcanol. 69, 51–56.

Witter, J.B., Kress, V.C., Newhall, C.G., 2005. Volcan Popocatepetl, Mexico. Petrology, magma mixing, and immediate sources of volatiles for the 1994–present eruption. J. Petrol. 46, 2337–2366.